Stabilisation of a non-collocated velocity feedback system by the use of inerter

N. Alujević [1], D. Čakmak [1], M. Jokić [1], H. Wolf [1]
[1] University of Zagreb, Faculty of Mechanical Engineering and Naval Architecture,
Ivana Lučića 5, 1000, Zagreb, Croatia
e-mail: **nalujevic@fsb.hr**

Abstract

In active vibration isolation systems direct velocity feedback may be used. A particular approach in this framework is known as "skyhook damping". Skyhook damping is implemented by using a velocity sensor mounted on the receiving body whose output is used to drive a force actuator reacting between the source and the receiving bodies through a feedback gain. In such an arrangement the velocity sensor is collocated with the component of the actuator force acting on the receiving body. The other component reacting against the source body lacks a collocated sensor. If the fundamental natural frequency of the receiving body is lower than the fundamental natural frequency of the source body, the feedback loop exhibits unconditional stability and can generate significant vibration isolation effects in a broad band of frequencies. If the situation is opposite, the feedback loop becomes conditionally stable and only limited feedback gains can be implemented. This results in poor vibration isolation effects. However, if an inerter with a large enough inertance is used in the isolator suspension, the feedback loop becomes unconditionally stable and performant again. In this paper it is calculated using a lumped parameter model of the general vibration isolation problem that the minimum inertance to stabilise the feedback loop equals the stiffness of the isolator spring times the squared natural frequency of the source body. Furthermore, it is shown that time-averaged kinetic energy of the receiving body monotonically reduces with the increase of the feedback gain.

1 Introduction

An appealing property of inerters is that they can be designed and realised in practice having their inertance significantly larger than their mass [1], [2]. Adding the inerter to classical dampers and springs fills an empty niche enabling a complete synthesis of passive mechanical networks [1], [2]. This opens many interesting possibilities so that many authors reported on how to design and use inerters to suppress mechanical vibrations [1]–[10].

For example, inerters can be very useful in vibration absorber systems. The performance of dynamic vibration absorbers is known to very much depend on the proof mass added to a primary structure to reduce its vibration. This mass is added to structures exclusively to control their vibrations, so it is penalised in lightweight automotive and aerospace applications [11]. In this context, the use of inerter elements can be interesting given the fact that their inertance can be significantly larger than their mass. Consequently a number of new concepts have arisen. These include tuned inerter damper (TID), tuned mass–damper–inerter (TMDI), and inerter–based dynamic vibration absorber (IDVA) [12]–[16]. In these systems the working frequency of the absorber can be tuned by changing the inertance. In particular, it can be reduced without increasing the physical mass of the vibration absorber while preserving the static stiffness of the absorber suspension spring. Various applications have been considered using tuned inerter dampers including vibration reduction of cables in cable-stayed bridges [13].

Dynamic vibration absorbers can be made active. Active vibration absorbers can be realised using proof-mass actuators implementing a velocity or velocity + displacement feedback control loop [17]–[21]. Normally, active vibration absorbers must be designed with a low mounted natural frequency [18], [19],

[22]. This requires either a large proof mass or soft suspension stiffness. Both is hard to realise in practice since the mass must not be too large as this would add too much weight to the structure, and the stiffness cannot be too small due to large sags in case of constant accelerations (gravity, vehicle manoeuvring). The need for soft suspension also limits the applicability of co-rotating proof-mass actuators for vibration control of structures rotating at a high speed which exposes the proof mass to large centrifugal forces [23]–[25]. This problem can be overcame by using an inerter between the proof mass and the structure under control. In such a way the natural frequency may be decreased without significantly increasing the weight of the system and without using excessively soft suspension springs.

Inerters can also be very useful in vibration isolation systems. In this sense, many authors focused their efforts on improving vehicle suspension systems using inerters [2], [29], [30]. Further applications of inerters include vibration isolation in civil engineering structures, such as multi-storey buildings under earthquake base excitation [31]. In vibration isolation problems it is often necessary to tune the impedance of the isolator elements based on some optimisation criteria. This can be done by either minimising maxima of the response (H_∞ optimisation), or by minimising the energy in the response signals (H_2 optimisation) [32].

In this paper the benefits of using inerter in an active vibration isolation problem are considered. It is shown that the use of an inerter in the isolator can significantly improve the stability and performance of the active vibration isolation system in certain situations. In particular, it is shown analytically on a simplified model problem that the use of inerter enables successful active vibration isolation in a family of mechanical systems that are otherwise difficult to control. This family of system has been referred to as subcritical 2 DOF systems. Subcritical systems are those characterised by the natural frequency of the receiving body larger than the natural frequency of the source body. In such vibration isolation problems the use of inerter is shown to stabilise the feedback loop and therefore to enable a remarkable active vibration isolation effect.

The paper is structured into three sections. In the second section, the model problem is presented and the corresponding mathematical formulation is given. In Section 3 a comprehensive stability analysis of the active vibration isolation scheme is given. This analysis indicates the subcritical family of vibration isolation systems that requires the use of inerters in the isolator to have stable and performant active vibration isolator. In Section 4 the performance of the active vibration isolation system is discussed through its ability to reduce the mean kinetic energy of the receiving body. In each system, tuneable parameters are adjusted in order to minimise the kinetic energy of the receiving body per unit, spectrally white, dynamic excitation of the source body.

2 Mathematical model

In this section mathematical model of an inerter-based active vibration isolation system is formulated. As shown in Figure 1, the problem studied is represented by a lumped parameter two degree of freedom (DOF) mechanical system. The system consists of two masses m_1 and m_2 coupled by a spring k_2, a viscous damper c_2 and an inerter of inertance b_2. The inerter produces a force proportional to the relative acceleration between masses m_1 and m_2. The two masses are attached to fixed reference bases via the two mounting springs k_1 and k_3. The lower mass m_1 is excited by the disturbance force F_1. It is assumed that the force F_1 has characteristics of an ideal white noise and that the power spectral density (PSD) of the force equals one over all frequencies.

The purpose of the vibration isolation system is to reduce vibrations of mass m_2 which are due to the forcing F_1 acting on mass m_1. Therefore, a structure approximated by mass m_1 and spring k_1 is referred to as the source body, and a structure characterised by the mass m_2 and stiffness k_3 is referred to as the receiving body (Figure 1).

Such a lumped parameter approximation may be representative of a system of more complicated nature, incorporating structures with distributed mass and stiffness parameters. For example, modal mass and stiffness of the fundamental mode of a flexible rectangular source panel can be represented through mass m_1 and stiffness k_1. Similarly, mass m_2 and stiffness k_3 can represent modal mass and stiffness corresponding to the fundamental mode of a flexible radiating panel. Finally, the stiffness k_2 between the two masses could represent a coupling impedance associated with the breathing mode of an air cavity between the two panels. In such a way the simplified 2 DOF model could be used to describe the low-frequency dynamic behaviour of acoustically coupled double panels as discussed in, for example [33]. Other systems may also be representable by the general configuration shown in Figure 1, such as those discussed in [17], [34]–[36]. In case a more detailed and accurate analysis is required, attention should be paid to the influence of higher order residual modes, see for example [6].

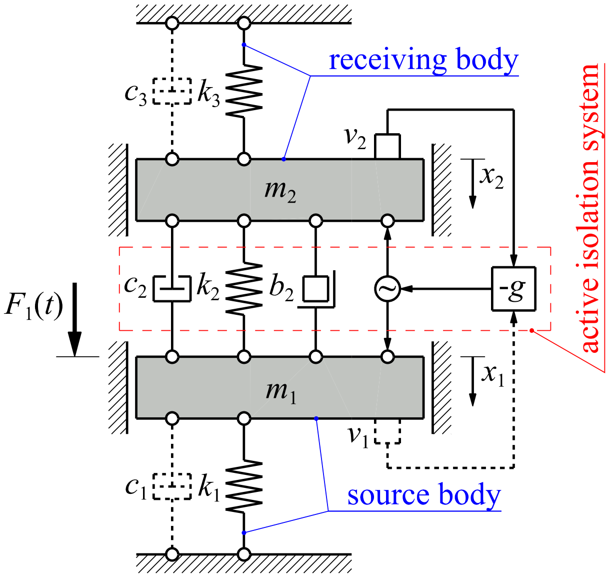

Figure 1. The two degree of freedom active vibration isolation system

The active part of the vibration isolation system is realised through a skyhook damping unit [35], [37]. The skyhook damper consists of a reactive actuator, a velocity sensor, and a feedback loop between the output of the sensor and the input to the actuator. The actuator is mounted in parallel with the passive part of the isolation system (spring, dashpot and inerter) with its terminals also attached to the two masses, Figure 1. The velocity sensor is mounted onto mass m_2 in order to realise a disturbance rejection control scheme. In this scheme the actuator is driven with a signal proportional to the negative absolute velocity of the receiving body amplified by a constant control gain g. Idealised sensor-actuator transducers are assumed. Thus the feedback gain g has physical dimension of Ns/m and could be referred to as the active damping coefficient. Practical velocity sensors are normally realized using standard accelerometers with time-integrated outputs. The cut-off frequency of the integration circuit is usually chosen low, so that in the frequency range between the cut-off frequency of the integrator and the blocked natural frequency of the accelerometer, the time-integrated output of the accelerometer is proportional to velocity [17], [18]. Also, an advanced MEMS velocity sensor with internal velocity feedback that could be used for this purpose has been proposed in [38].

The actuator force F_A is given by

$$F_A = -g\dot{x}_2 . \tag{1}$$

The equations of motion are

$$\begin{aligned}(m_1+b_2)\ddot{x}_1 - b_2\ddot{x}_2 + c_2\dot{x}_1 - (c_2+g)\dot{x}_2 + (k_1+k_2)x_1 - k_2x_2 = F_1 \\ -b_2\ddot{x}_1 + (m_2+b_2)\ddot{x}_2 - c_2\dot{x}_1 + (c_2+g)\dot{x}_2 - k_2x_1 + (k_2+k_3)x_2 = 0\end{aligned} . \tag{2a,b}$$

Equations of motion Eq. (2a,b) can be written in the matrix form as

$$\mathbf{M}\ddot{\mathbf{x}} + \mathbf{C}\dot{\mathbf{x}} + \mathbf{K}\mathbf{x} = \mathbf{F} , \tag{3}$$

where $\mathbf{M}$ is the mass matrix, $\mathbf{K}$ is the stiffness matrix, $\mathbf{C}$ is the damping matrix, $\mathbf{x}(t)$, $\dot{\mathbf{x}}(t)$ and $\ddot{\mathbf{x}}(t)$ are the displacement, velocity and acceleration column vectors respectively, and $\mathbf{F}(t)$ is excitation column vector. These matrices/vectors are given by the following expressions

$$\mathbf{M}=\begin{bmatrix} m_1+b_2 & -b_2 \\ -b_2 & m_2+b_2 \end{bmatrix},\quad \mathbf{C}=\begin{bmatrix} c_1+c_2 & -c_2-g \\ -c_2 & c_2+c_3+g \end{bmatrix},\quad \mathbf{K}=\begin{bmatrix} k_1+k_2 & -k_2 \\ -k_2 & k_2+k_3 \end{bmatrix}, \tag{4a-c}$$

$$\mathbf{x}=\begin{bmatrix} x_1(t) \\ x_2(t) \end{bmatrix},\quad \mathbf{F}=\begin{bmatrix} F_1(t) \\ 0 \end{bmatrix}, \tag{5a-b}$$

where the parameters/functions in the matrices/vectors are as indicated in Figure 1. Note that the gain g generates diagonally asymmetric active damping terms in the system damping matrix $\mathbf{C}$. Throughout this study, the damping of the source and receiving structures is assumed to be light. Thus the effects of dampers between the source mass m_1 and the ground and between the receiving mass m_2 and the ground are neglected *i.e.* $c_1 \approx c_3 \approx 0$. This enables significantly less complex mathematical derivations in the forthcoming parts of the study. Furthermore it leads to a more transparent model regarding the physics governing the system dynamical behaviour.

Assuming a simple harmonic excitation and expressing the excitation and the steady-state response in the exponential form $\mathbf{F}(t)=\hat{\mathbf{F}}e^{\mathrm{j}\omega t}$ and $\mathbf{x}=\hat{\mathbf{x}}e^{\mathrm{j}\omega t}$, where $\mathrm{j}=\sqrt{-1}$, Eq. (3) can be written as

$$\mathbf{S}(\mathrm{j}\omega)\mathbf{x}(\mathrm{j}\omega)=\mathbf{F}(\mathrm{j}\omega), \tag{6}$$

where $\mathbf{S}(\mathrm{j}\omega)$ is the dynamic stiffness matrix with the following form

$$\mathbf{S}(\mathrm{j}\omega)=-\omega^2\mathbf{M}+\mathrm{j}\omega\mathbf{C}+\mathbf{K}\,. \tag{7}$$

Solution of Eq. (6) can be obtained by inversion of the dynamic stiffness matrix $\mathbf{S}(\mathrm{j}\omega)$ as

$$\mathbf{x}(\mathrm{j}\omega)=\mathbf{S}^{-1}(\mathrm{j}\omega)\mathbf{F}(\mathrm{j}\omega)\,. \tag{8}$$

Differentiating Eq. (8) in order to obtain velocities results in expression

$$\dot{\mathbf{x}}(\mathrm{j}\omega)=\mathbf{Y}(\mathrm{j}\omega)\mathbf{F}(\mathrm{j}\omega), \tag{9}$$

where $\dot{\mathbf{x}}(\mathrm{j}\omega)=\mathrm{j}\omega\,\mathbf{x}(\mathrm{j}\omega)$ is the velocity vector and $\mathbf{Y}(\mathrm{j}\omega)=\mathrm{j}\omega\,\mathbf{S}^{-1}(\mathrm{j}\omega)$ is the mobility matrix representing four frequency response functions (FRFs) between velocities and forces. By taking $\mathbf{M}$, $\mathbf{K}$ and $\mathbf{C}$ matrices from Eq. (4a-c), the steady-state complex response can be expressed in terms of the two driving points and two transfer mobilities as

$$Y_{11}(\mathrm{j}\omega)=\frac{(\mathrm{j}\omega)^3(m_2+b_2)+(\mathrm{j}\omega)^2(c_2+g)+(\mathrm{j}\omega)(k_2+k_3)}{\begin{gathered}(\mathrm{j}\omega)^4\left[(b_2+m_2)m_1+b_2m_2\right]+(\mathrm{j}\omega)^3\left[(c_2+g)m_1+c_2m_2\right]+\\+(\mathrm{j}\omega)^2\left[(m_2+b_2)k_1+(m_1+m_2)k_2+(m_1+b_2)k_3\right]+(\mathrm{j}\omega)\left[(c_2+g)k_1+c_2k_3\right]+(k_2+k_3)k_1+k_2k_3\end{gathered}}, \tag{10a}$$

$$Y_{12}(\mathrm{j}\omega)=\frac{(\mathrm{j}\omega)^3 b_2+(\mathrm{j}\omega)^2(c_2+g)+(\mathrm{j}\omega)k_2}{\begin{gathered}(\mathrm{j}\omega)^4\left[(b_2+m_2)m_1+b_2m_2\right]+(\mathrm{j}\omega)^3\left[(c_2+g)m_1+c_2m_2\right]+\\+(\mathrm{j}\omega)^2\left[(m_2+b_2)k_1+(m_1+m_2)k_2+(m_1+b_2)k_3\right]+(\mathrm{j}\omega)\left[(c_2+g)k_1+c_2k_3\right]+(k_2+k_3)k_1+k_2k_3\end{gathered}}, \tag{10b}$$

$$Y_{21}(\mathrm{j}\omega)=\frac{(\mathrm{j}\omega)^3 b_2+(\mathrm{j}\omega)^2 c_2+(\mathrm{j}\omega)k_2}{\begin{array}{c}(\mathrm{j}\omega)^4\left[(b_2+m_2)m_1+b_2m_2\right]+(\mathrm{j}\omega)^3\left[(c_2+g)m_1+c_2m_2\right]+\\+(\mathrm{j}\omega)^2\left[(m_2+b_2)k_1+(m_1+m_2)k_2+(m_1+b_2)k_3\right]+(\mathrm{j}\omega)\left[(c_2+g)k_1+c_2k_3\right]+(k_2+k_3)k_1+k_2k_3\end{array}}, \tag{10c}$$

$$Y_{22}(\mathrm{j}\omega)=\frac{(\mathrm{j}\omega)^3 (m_1+b_2)+(\mathrm{j}\omega)^2 c_2+(\mathrm{j}\omega)(k_1+k_2)}{\begin{array}{c}(\mathrm{j}\omega)^4\left[(b_2+m_2)m_1+b_2m_2\right]+(\mathrm{j}\omega)^3\left[(c_2+g)m_1+c_2m_2\right]+\\+(\mathrm{j}\omega)^2\left[(m_2+b_2)k_1+(m_1+m_2)k_2+(m_1+b_2)k_3\right]+(\mathrm{j}\omega)\left[(c_2+g)k_1+c_2k_3\right]+(k_2+k_3)k_1+k_2k_3\end{array}}, \tag{10d}$$

where $Y_{ij}=\dot{x}_i/F_j$ is a mobility function of the system, representing a velocity of the mass i due to a unit force at the mass j. If $i = j$ then the corresponding FRF is referred to as a driving point mobility, otherwise it is a referred to as a transfer mobility.

The transfer mobility Y_{21}, representing the velocity response of the receiving body per unit forcing of the source body, is used to assess the quality of the vibration isolation throughout this paper. With the aim of more general approach, mobility Y_{21} in Eq. (10c) can be expressed in the following dimensionless form

$$\Upsilon_{21}(\mathrm{j}\Omega)=\frac{B_0+(\mathrm{j}\Omega)B_1+(\mathrm{j}\Omega)^2 B_2+(\mathrm{j}\Omega)^3 B_3}{A_0+(\mathrm{j}\Omega)A_1+(\mathrm{j}\Omega)^2 A_2+(\mathrm{j}\Omega)^3 A_3+(\mathrm{j}\Omega)^4 A_4}, \tag{11}$$

where coefficients $A_0...A_4$ and $B_0…B_3$ are given by

$$\begin{array}{ll} A_0=\mu_1(\alpha\beta\mu_1+\alpha+\beta) & B_0=0 \\ A_1=2\eta_2(\beta\mu_1+\lambda+1) & B_1=\alpha\mu_1 \\ A_2=\mu_1(\alpha\mu_1+\beta\mu_1\mu_2+\alpha+\beta+\mu_2+1) & B_2=2\eta_2 \\ A_3=2\eta_2(\mu_1+\lambda+1) & B_3=\mu_1\mu_2 \\ A_4=\mu_1(\mu_1\mu_2+\mu_2+1) & \end{array}, \tag{12a-i}$$

where

$$\alpha=\left(\frac{\Omega_2}{\Omega_1}\right)^2,\quad \beta=\left(\frac{\Omega_3}{\Omega_1}\right)^2,\quad \eta_2=\frac{c_2}{2\sqrt{m_1k_1}},\quad \lambda=\frac{g}{c_2},\quad \mu_1=\frac{m_2}{m_1},\quad \mu_2=\frac{b_2}{m_2},\quad \Omega=\frac{\omega}{\Omega_1}, \tag{13a-g}$$

and $\Upsilon_{21}=m_1\Omega_1Y_{21}$ is now the dimensionless transfer mobility. Throughout the rest of the paper, it is assumed that m_1 and Ω_1 are constant values, used for scaling the transfer mobility function Y_{21} to convenient dimensionless form. In Eqs. (13a-g), α and β are squared natural frequency ratios, η_2 is the damping ratio, λ is the feedback gain normalised with respect to the passive damping coefficient, and μ_1 and μ_2 are the mass and inertance ratios respectively. Furthermore, Ω is dimensionless circular frequency normalised with respect to the natural frequency of the uncoupled source body Ω_1 (as if the source body was uncoupled by removing spring k_2), Ω_3 is the natural frequency of the uncoupled receiving body (as if the receiving body was uncoupled by removing spring k_2), and Ω_2 is the natural frequency of the receiving body as if it was attached to a fixed reference base through the spring of stiffness k_2 only. The three natural frequencies $\Omega_1…\Omega_3$ are thus

$$\Omega_1=\sqrt{\frac{k_1}{m_1}},\quad \Omega_2=\sqrt{\frac{k_2}{m_2}},\quad \Omega_3=\sqrt{\frac{k_3}{m_2}}. \tag{14a-c}$$

Given that the excitation force F_1 with unit PSD has been assumed, the specific kinetic energy of the receiving body (per unit mass, per unit excitation force) can be calculated as

$$I_k = \int_{-\infty}^{\infty} \left| \varUpsilon_{21}(\mathrm{j}\varOmega) \right|^2 \mathrm{d}\varOmega, \tag{15}$$

The specific kinetic energy index I_k is used throughout this study as a measure of the performance of broad frequency band vibration isolation. The objective of the active vibration isolation system is to minimise this quantity.

The specific kinetic energy index in Eq. (15) can according to [39] be calculated as

$$I_k = \pi \frac{A_0 B_3^2 \left(A_0 A_3 - A_1 A_2\right) + A_0 A_1 A_4 \left(2 B_1 B_3 - B_2^2\right) - A_0 A_3 A_4 \left(B_1^2 - 2 B_0 B_2\right) + A_4 B_0^2 \left(A_1 A_4 - A_2 A_3\right)}{A_0 A_4 \left(A_0 A_3^2 + A_1^2 A_4 - A_1 A_2 A_3\right)}. \tag{16}$$

Substituting coefficients $A_0 ... A_4$ and $B_0 \dots B_3$ from Eq. (12) into Eq. (16) yields

$$I_k = 2\pi \frac{\left(\begin{array}{c} 1/4\mu_2\left(\mu_2\beta-\alpha\right)^2\mu_1^{\,4} + 1/4\left(\mu_2\beta-\alpha\right)\left[\left(\lambda+2\right)\mu_2^{\,2} + \left(\beta-\alpha\lambda-2\alpha\right)\mu_2 - \alpha\right]\mu_1^{\,3} + \\ +\left\{ \begin{array}{c} 1/4\left(1+\lambda\right)\mu_2^{\,3} - 1/2\left(-1/2+\alpha\right)\left(\lambda+1\right)\mu_2^{\,2} + \\ +\left[\left(1/4\alpha^2 - 1/2\alpha\right)\lambda + \beta\eta_2^2 + 1/4\alpha^2 - 1/2\alpha\right]\mu_2 + 1/4\alpha^2\left(\lambda+1\right) \end{array} \right\}\mu_1^{\,2} + \\ +\left[\left(1+\beta+\lambda\right)\mu_2 + \beta\right]\eta_2^2\mu_1 + \eta_2^2\left(1+\mu_2\right)\left(\lambda+1\right) \end{array} \right)}{\eta_2\left(1+\mu_2+\mu_2\mu_1\right)\left(\beta-1\right)\left[\lambda\left(\mu_2\beta-\alpha\right)\mu_1 + \left(\lambda+1\right)\left(\lambda\mu_2 - \alpha\lambda + \beta - 1\right)\right]\mu_1^{\,2}}. \tag{17}$$

In the remaining parts of the paper, two types of vibration isolation systems are studied and compared with respect to their performance in minimising the kinetic energy index I_k. These are the active control system without inerter and the active control system with inerter. First, stability properties of the feedback loop are discussed for the two types of active vibration isolation systems: without and with the inerter. Second, the performance of the two active vibration isolation systems are analysed.

3 Stability

3.1 Stability in general

With the frequency domain analysis, the stability of active control systems cannot be seen directly from the frequency response of the system. In other words, the model presented in Section 2 mathematically allows for calculating frequency response functions using Eqs. (10) for both stable and unstable systems. However, such FRFs for unstable systems would be physically meaningless. It is thus necessary to carefully investigate the active control system stability properties before calculating the prospective performance metrics, such as the kinetic energy index given by Eq. (16). It has previously been shown that active vibration isolation systems can exhibit stability problems as discussed in for example [17], [34], [40], [41]. In this subsection, the stability of the feedback control loop is studied with reference to the dimensionless active damping coefficient λ by applying the Routh-Hurwitz stability criterion to the characteristic equation of the system. The characteristic equation is the denominator of Eq. (11).

According to the Routh-Hurwitz necessary stability condition and Eq. (12) in order for $A_{1,3} > 0$, it must be

$$\forall\beta < 1 \;\Rightarrow\; \lambda > -\left(\beta\mu_1 + 1\right) \text{ in order for } A_1 > 0, \tag{18}$$

$$\forall\beta > 1 \;\Rightarrow\; \lambda > -\left(\mu_1 + 1\right) \text{ in order for } A_3 > 0. \tag{19}$$

In other words, if $\beta < 1$ the condition $A_1 > 0$ is a stricter one and if $\beta > 1$, then $A_3 > 0$ is the stricter condition. Considering now the Routh-Hurwitz sufficient condition for stability, it states that all diagonal sub-determinants H_1, H_2 and H_3, as well as the main determinant H_4 of Hurwitz matrix must be positive. The principal determinant H_4 is proportional to the sub-determinant H_3 with an always positive term $\mu_1(\alpha(\beta\mu_1+1)+\beta)$ and is thus automatically positive if H_3 is positive. Thus the relevant criteria that must be satisfied simultaneously are Eqs. (18) and (19) plus the following additional ones

$$H_1 > 0 \;\Rightarrow\; \lambda + \mu_1 + 1 > 0, \tag{20}$$

$$H_2 > 0 \;\Rightarrow\; 2\mu_1\eta_2\left\{\left[\mu_1\left(\mu_2(\beta-1)+\alpha\right)\lambda+\alpha+\beta\right]+\mu_1\left[1+\alpha(2+\mu_1)\right]+\alpha+\beta\right\} > 0, \tag{21}$$

$$H_3 > 0 \;\Rightarrow\; 4\mu_1^2\eta_2^2(\beta-1)\left\{(\mu_2-\alpha)\lambda^2+\left[\beta\mu_2(\mu_1+1)+\beta-1-\alpha(\mu_1+1)\right]\lambda+\beta-1\right\} > 0. \tag{22}$$

Note that A_1, A_3, H_1 and H_2 are linear functions of the dimensionless feedback gain λ, whereas H_3 is a quadratic function of λ. The quadratic determinant H_3 changes sign at the following values of the feedback gain

$$\lambda_{1,2} = \frac{\mu_2(\beta\mu_1+1)-\alpha(\mu_1+1)+\beta-1\mp\sqrt{(\alpha-\mu_2\beta)^2\mu_1^2+2\mu_1(\alpha-\mu_2\beta)(\alpha+1-\mu_2-\beta)+(\alpha-\mu_2+\beta-1)^2}}{2(\alpha-\mu_2)}. \tag{23a,b}$$

In the forthcoming discussion, it is shown that by ensuring the validity of inequality (22), all other stability conditions are satisfied automatically. In other words, the condition (22) is a *sufficient* stability condition for the problem studied.

3.2 Stability without inerter – subcritical and supercritical systems

If the inerter is not used, *i.e.* $\mu_2 = 0$, Eqs. (23a,b) can be simplified to

$$\lambda_{1,2} = \frac{\beta-1-\alpha(\mu_1+1)\mp\sqrt{(1+\mu_1)^2\alpha^2-2(\mu_1-1)(\beta-1)\alpha+(\beta-1)^2}}{2\alpha}, \tag{24a,b}$$

where λ_1 is the lower value out of two zeros. At this point it is convenient to graphically represent all expressions relevant for the system stability as a function of the dimensionless feedback gain λ. This is done in Figure 2. Two different cases are presented. Figure 2(a) shows the case when the squared natural frequency ratio $\beta < 1$ and Figure 2(b) shows the case with $\beta > 1$.

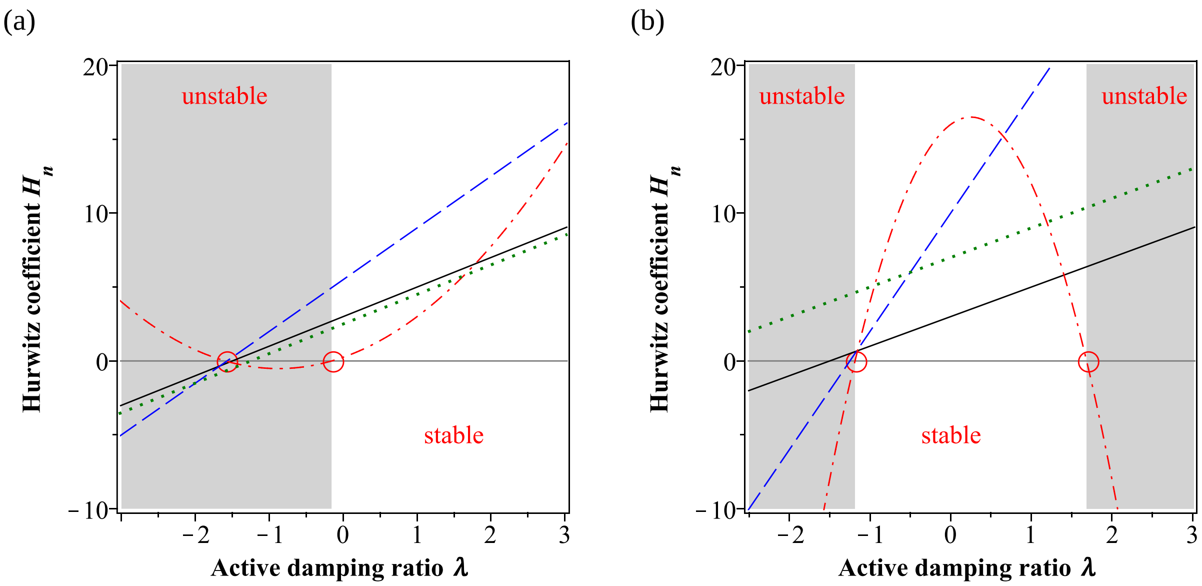

Figure 2: Hurwitz coefficients H_1 (solid line), H_2 (dashed line), H_3 (dash-dotted line) and A_1 (dotted line) plotted against the active damping ratio λ without inerter: (a) $\beta < 1$, (b) $\beta > 1$

The parameters of an example system shown in Figure 2(a) are $\alpha = 2$, $\mu_1 = 1/2$, $\eta_2 = 1$ and $\beta_{(a)} = 1/2$, and the parameters for an example system shown in Figure 2(b) are the same, except $\beta_{(b)} = 5$. The zeros of the 3rd principal diagonal minor H_3 from Eqs. (24a,b) are denoted by the two circles. In both plots can be seen that if the principal diagonal minor with the quadratic dependence on the feedback gain is positive, *i.e.* $H_3 > 0$, then all other stability conditions are automatically satisfied. In fact, by closely inspecting Eqs. (18-22) it could be deduced that it is generally true that if $H_3 > 0$ then all other conditions, *i.e.* Eqs. (18-21), are automatically satisfied and the stability is guaranteed. Thus Eq. (22) represents the strictest stability condition and it becomes sufficient to make sure that $H_3 > 0$ in order to have a stable feedback loop.

Physically this indicates that if the uncoupled natural frequency of the source body is larger than the uncoupled natural frequency of the receiving body, then a negative velocity feedback loop with an arbitrary large feedback gain can be used. As discussed in the forthcoming Section 4.1, this is a situation in which very convincing active vibration isolation effects can be achieved. On the other hand, in situation in which the uncoupled natural frequency of the source body is smaller than the uncoupled natural frequency of the receiving body, as shown in Figure 2(b), the range of dimensionless feedback gains is limited between λ_1 and λ_2, according to Eq. 24. Therefore, the maximum feedback gain is limited by λ_2 above which the second order principal diagonal minor becomes negative with further increasing the feedback gain. This is because the parabola in Figure 2(b) is oriented downwards whereas the parabola in Figure 2(a) is oriented upwards. This situation results in a limited active vibration control performance as discussed in the forthcoming section 4.1.

In conclusion, it can be stated that all systems representable by the scheme in Figure 1 can be divided into two families. The first family can be referred to as *supercritical* and it is characterised by $\beta < 1$. The systems belonging to this group allow for the implementation of unconditionally stable active vibration isolation scheme based on the direct feedback of the absolute velocity of the receiving body. The second family is characterised by $\beta > 1$ and it can be referred to as *subcritical*. The systems belonging to this group do not allow for the implementation of unconditionally stable absolute velocity feedback scheme. On the contrary, the feedback loop is conditionally stable with a limited maximum feedback gain.

Practical vibration isolation problems belonging to the supercritical family are the problems of isolating vibrations coming from a flexible base towards sensitive equipment mounted on the base. A practical problem belonging to the subcritical group could be a problem in which running machinery is elastically mounted on the flexible base, for example a punching press. In such case, the broadband vibrations originating from the impact, transmit from the machine to the base. It appears from the above analysis that it would be significantly more difficult to guarantee the stability of the absolute velocity feedback control applied on the latter, subcritical family of vibration isolation problems. Given these difficulties, it is interesting to investigate the effects of the use of an inerter with subcritical systems characterised by $\beta > 1$. This investigation is carried out in the following subsection.

3.3 Stability with inerter – stabilising the feedback loop in a subcritical system

If an inerter is used in an isolator of a subcritical system characterised by $\beta > 1$, then interesting effects can be observed with regard to the stability of the feedback loop. By inspecting Eq. (22), it can be seen that the third principal diagonal minor H_3, which is essential for the stability of the active control, has the quadratic coefficient in λ equal to $\mu_2 - \alpha$. This coefficient determines whether the corresponding parabola is pointing upwards or downwards. Given that the term $(\beta - 1)$ multiplying the squared bracket expression is positive with subcritical systems, it turns out that an inerter with dimensionless inertance $\mu_2 > \alpha$ can make the quadratic coefficient of the parabola positive. This in turn results in an upward pointing parabola. Therefore unconditional stability can be achieved also with subcritical systems simply by adding an inerter with $\mu_2 > \alpha$. This is illustrated in Figure 3 which shows all principal diagonal minors calculated according to Eqs. (20 -22). The system is again characterised by $\alpha = 2$, $\mu_1 = 1/2$, $\eta_2 = 1$ and $\beta = 5$, just like in Figure 2(b). As shown in Figure 3(a), with the inclusion of inerter when $\beta > 1$ and $\mu_{2(a)} = \alpha/2$, the limited stable range of λ between $\lambda_{H1} < \lambda < \lambda_{H2}$, is expanded in comparison with Figure 2(b). If the inertance is further increased, so that $\mu_2 = 2\alpha$, the system becomes stable for any $\lambda > \lambda_{H2}$, as shown in Figure 3(b). Therefore, for subcritical systems where the fundamental natural frequency of the receiving body is larger than that of the source body, the use of inerter characterised by $\mu_2 > \alpha$ drastically improves the stability by turning a subcritical active vibration isolation problem into a supercritical one. This is quite essential for the performance of the active vibration isolation, as discussed in the following Section 4.

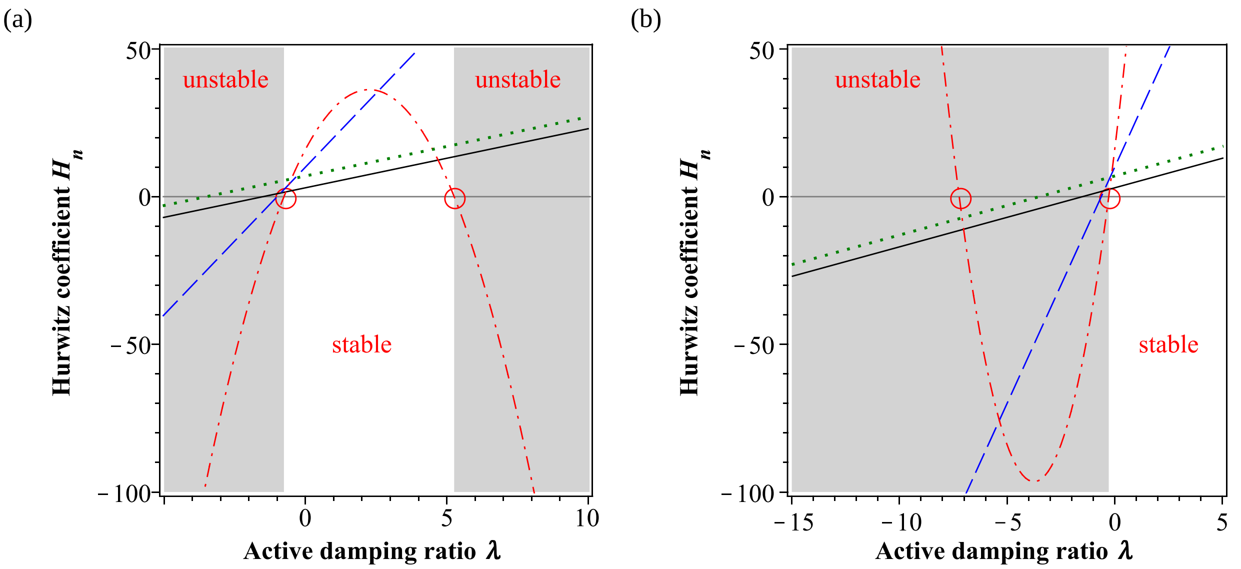

Figure 3: Hurwitz coefficients H_1 (solid line), H_2 (dashed line), H_3 (dash-dotted line) and A_1 (dotted line) plotted against the active damping ratio λ with inerter and with $\beta > 1$: (a) $\mu_2 < \alpha$, (b) $\mu_2 > \alpha$

4 Performance

4.1 Without inerter

The performance of the active control is first studied without the use of inerter, therefore dimensionless parameter μ_2 equals zero. Figure 4(a) shows the specific kinetic energy index of the receiving body plotted as a function of the passive and active damping ratio.

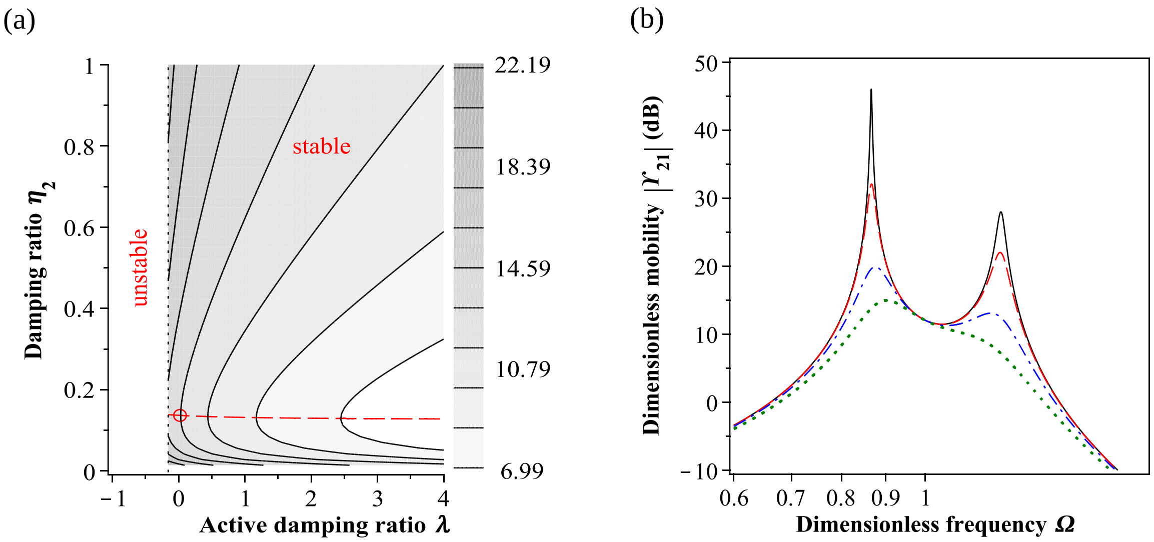

Figure 4. Active vibration isolation system performance without inerter b_2 ($\mu_2 = 0$) and $\beta < 1$: (a) Specific kinetic energy index I_k, (b) Transfer mobility function $\left|\varUpsilon_{21}(\mathrm{j}\varOmega)\right|$, $\lambda = 0$ (solid line), $\lambda = 2$ (dashed line), $\lambda = 10$ (dash-dotted line), $\lambda = 20$ (dotted line)

Firstly, a supercritical system is assumed so the frequency ratio β is smaller than one. Figure 4(a) indicates that as the active damping ratio (the feedback gain) is increased, the kinetic energy index monotonically decreases demonstrating that the desired active vibration isolation effect is achieved. Figure 4(b) shows the dimensionless transfer mobility function (the velocity of the receiving body per unit forcing of the source body, as a function of frequency) for increasing active damping ratios. It can be seen that the amplitude of the dimensionless transfer mobility function $\left|\Upsilon_{21}(\mathrm{j}\Omega)\right|$ diminishes in the vicinity of Ω_{n1} and Ω_{n2} which is tied to significant reduction of the receiving body specific kinetic energy I_k. In addition, no increase of the amplitude of the mobility with an increase in the feedback gain can be seen at any frequency. Thus a true broadband active vibration isolation effect can be achieved. The characteristic parameters of the example system illustrated in Figure 4(a) are $\alpha = 1/2$, $\beta = 1/2$ and $\mu_1 = 1/2$. Parameters of the example system shown in Figure 4(b) are the same, except that the damping ratio had to be fixed to $\eta_2 = 0.5$ %. Therefore in such a supercritical system, the use of inerter appears to be unnecessary, since the system is stable for any given positive value of λ.

Considering now the subcritical case, where $\beta > 1$, the system is stable for a limited narrow λ - range as already discussed in Section 3.1 and as shown in Figure 2(b). Therefore it is interesting to investigate into performance of the active control for subcritical systems when the stable feedback gain is restricted between the lower and upper margins shown in Figure 2(b).

The kinetic energy index of the receiving body in this case ($\beta > 1$) is shown in Figure 5(a). The parameters of the example system shown in Figure 5(a) are $\alpha = 1/2$, $\beta = 2$ and $\mu_1 = 1/2$. It can be seen the figure that there is an optimum combination of the passive and active damping ratios that minimises the kinetic energy index which is marked by the red circle.

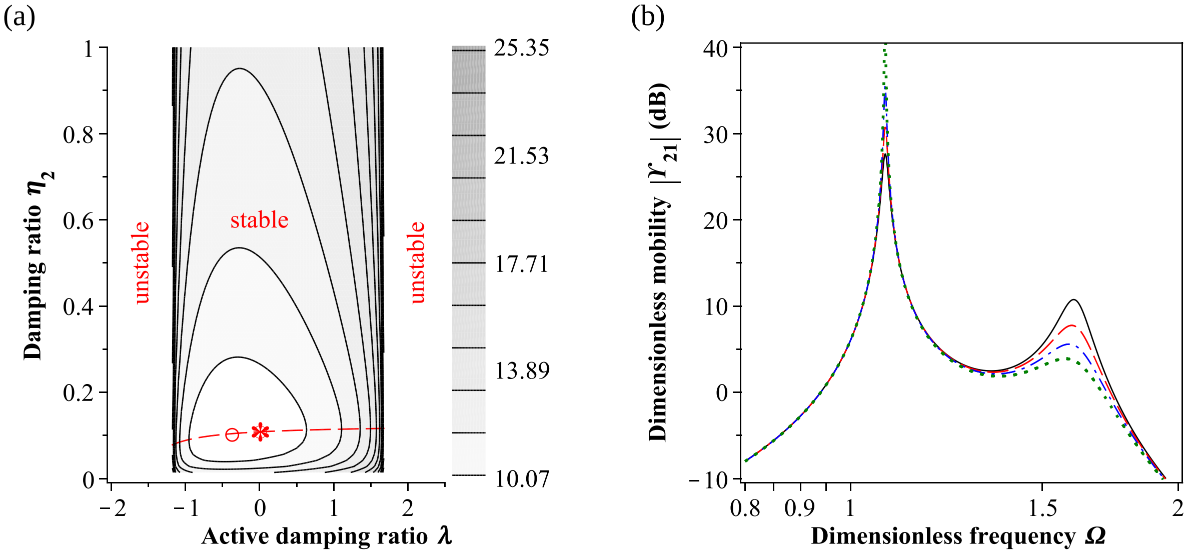

Figure 5: Active vibration isolation system performance without inerter b_2 ($\mu_2 = 0$) and $\beta_{\mathrm{II}} > 1$: (a) Specific kinetic energy index I_k, (b) Transfer mobility function $\left|\Upsilon_{21}(\mathrm{j}\Omega)\right|$, $\lambda = 0$ (solid line), $\lambda = 0.5$ (dashed line), $\lambda = 1$ (dash-dotted line), $\lambda = 1.5$ (dotted line)

The optimum passive damping ratio as a function of the active damping ratio is shown by the red dashed line in the plot (a). This function can be calculated by differentiating Eq. (17) with respect to λ and equalling with zero which yields the following relation:

$$\eta_{2\mathrm{opt},\lambda} = \frac{\alpha\mu_1}{2}\sqrt{\frac{1+\mu_1+\lambda}{1+\beta\mu_1+\lambda}}. \tag{25}$$

Eq. (25) is denoted by the dashed line in Figure 5(a). By substituting Eq. (25) into Eq. (17), the expression for minimum specific kinetic energy along the dashed line can be obtained

$$I_{k\min} = 2\pi \frac{\alpha\sqrt{(\beta\mu_1+\lambda+1)(\mu_1+\lambda+1)}}{\mu_1(\beta-1)\left[(-1+\beta-\mu_1\alpha-\alpha)\lambda-1+\beta-\alpha\lambda^2\right]}. \tag{26}$$

By differentiating Eq. (26) with respect to λ, equalling with zero and solving for λ, optimal active damping coefficient λ_{opt} may be obtained. Inserting both $\eta_{2opt,\lambda}$ from Eq. (25) and λ_{opt} into Eq. (17) yields an expression for minimum specific kinetic energy I_k. However, the relations for λ_{opt}, $\eta_{2opt,}$ and I_k are too cumbersome and not easily interpretable, so they are omitted here. Nevertheless, the global minimum position for I_k with respect to two variables λ_{opt} and $\eta_{2opt,\lambda 2}$ exists and it is denoted by the circle in contour plot. The asterisk in Figure 5.(a) denotes the minimum kinetic energy index if value of λ is set to zero, which implies the use of optimised passive control. By comparing the surface levels in Figure 5(a) at the optimum active control (circle) and the optimum passive control (asterisk) it can be seen that the level difference is about one dB. Therefore, the active control can outperform the passive control, but the corresponding improvement in performance is not particularly convincing. It can be concluded that with subcritical system the performance of the active vibration scheme is questionable, since a significantly simpler passive system can achieve nearly the same vibration isolation effect. The reasons for this are further investigated by plotting the dimensionless transfer mobility $|\Upsilon_{21}(\mathrm{j}\Omega)|$ as a function of frequency for cases with no control (λ = 0) and with the active control using increasing active damping ratios (increasing feedback gains) in Figure 5(b). The parameters for the example system shown in Figure 5(b) are the same as those in Figure 5(a), except that a fixed passive damping ratio $\eta_2 = 0.02$ is used. It can be seen in Figure 5(b), that although the amplitude of the dimensionless mobility $|\Upsilon_{21}(\mathrm{j}\Omega)|$ reduces in the vicinity of second natural frequency Ω_{n2} with rising λ, a significant overshoot can be observed in the vicinity of first natural frequency Ω_{n1} for rising λ. Figure 5(a) shows that for rising λ, the specific kinetic energy I_k also rises significantly until instability occurs. Therefore, using active control without inerter in cases when $\beta > 1$ results in generally doubtful performance. Figure 6(b) shows the comparison between the optimum active vibration isolation and the optimum passive vibration isolation for a subcritical system characterised by α = 1/2, β = 2 and μ_1 = 1/2 in terms of the amplitude of the transfer mobility plotted as a function of frequency.

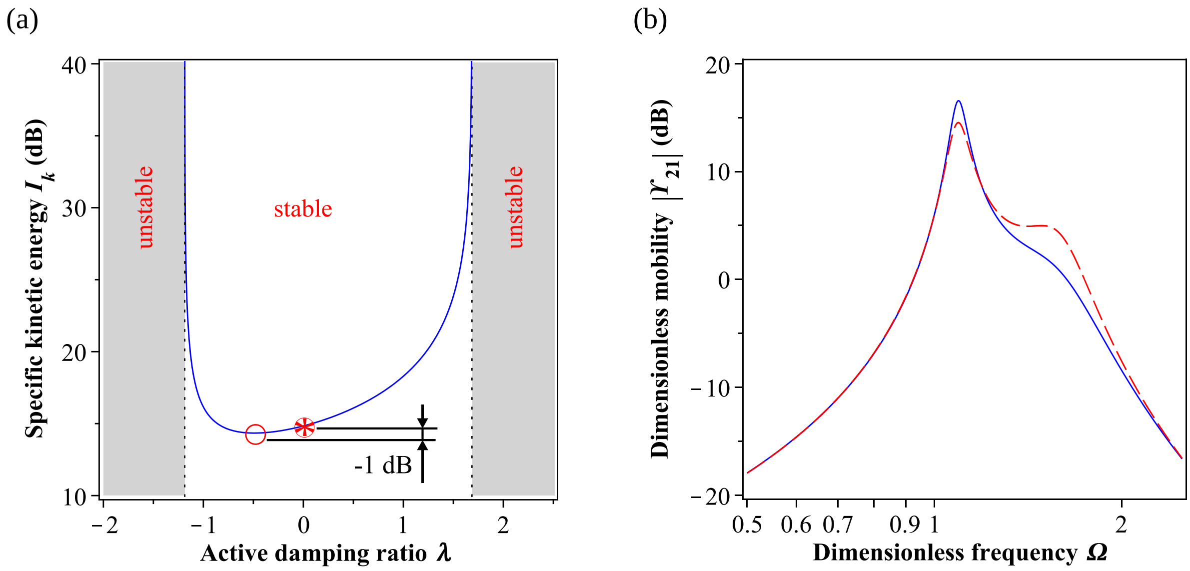

Figure 6: Active vibration isolation system performance without inerter b_2 (μ_2 = 0) and $\beta > 1$: (a) Specific kinetic energy index I_k, (b) Transfer mobility function $|\Upsilon_{21}(\mathrm{j}\Omega)|$, λ = 0, $\eta_2 = \eta_{2opt1}$ (solid line), $\lambda = \lambda_{opt}$, $\eta_2 = \eta_{2opt}$ (dashed line)

The same parameters are used in Figure 6(a) where the passive damping ratio is set to η_2 = 0.02. The optimised active control results in a slightly lesser kinetic energy index compared to the optimised passive control, which is obtained by damping down the velocity response around the first natural frequency at the expense of slightly increasing the response around the second natural frequency, Figure 6 (b). However, the improvement in performance due to the use of active control probably does not justify the complexity of the active vibration isolation system.

4.2 With inerter

Figure 7(a) shows the specific kinetic energy I_k of the receiving body plotted as a function of the active damping ratio λ of a subcritical system characterised by $\alpha = 1/2$, $\beta = 2$, $\mu_1 = 1/2$ and $\eta_2 = 0.01$, equipped with an inerter of inertance $\mu_2 = 2$. Therefore an inertance large enough to stabilise the feedback loop is used ($\mu_2 > \alpha$). It can be seen that with an increase in the dimensionless feedback gain λ, the specific kinetic energy index monotonically decreases indicating that the desired vibration isolation effect is accomplished.

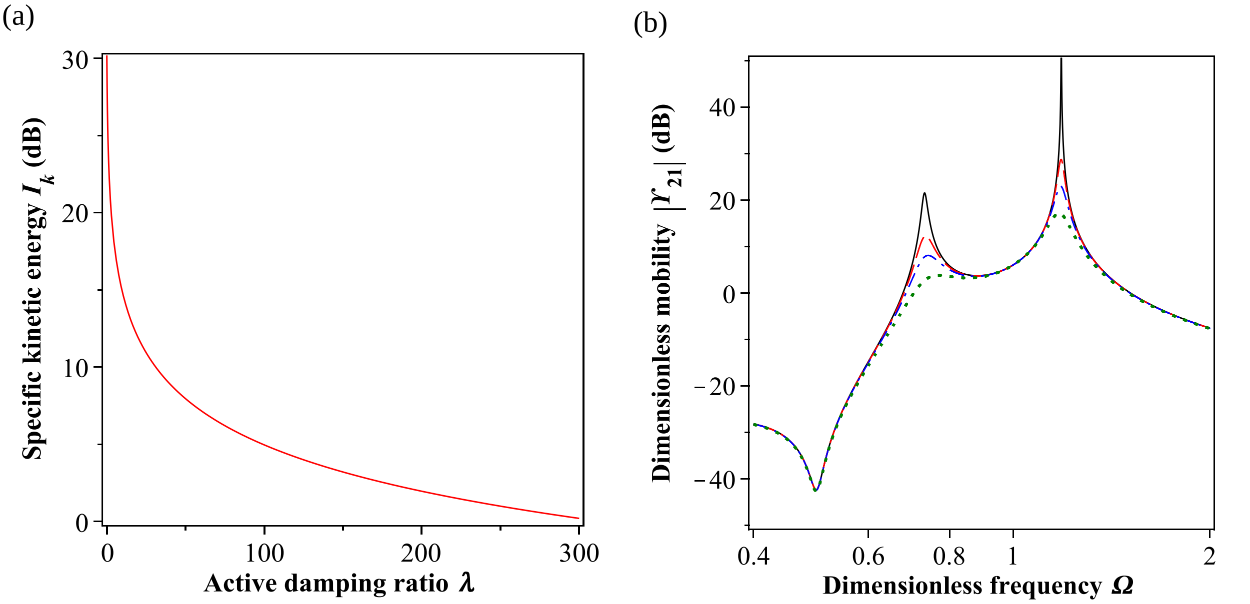

Figure 7: Active vibration isolation system performance with inerter b_2 ($\mu_2 \neq 0$), $\beta > 1$ and $\mu_2 > \alpha$: (a) Specific kinetic energy index I_k, (b) Transfer mobility function $|\Upsilon_{21}(\mathrm{j}\Omega)|$, $\lambda = 0$ (solid line), $\lambda = 5$ (dashed line), $\lambda = 10$ (dash-dotted line), $\lambda = 20$ (dotted line)

Figure 7(b) shows the amplitude of the dimensionless transfer mobility plotted against frequency for increasing feedback gains. Note the anti-resonance effect at frequencies below the first resonance, introduced by inerter. It can be seen that with the increase in the feedback gain, the receiving body response is decreased at either resonance frequency. The higher the gain, the lower is the velocity response. There can be seen no frequencies at which the increase of the feedback gain causes an increase of the response. Therefore, it can be concluded that the inclusion of the inerter in the active vibration isolation scheme with subcritical problems is essential in establishing stable and efficient active vibration isolation. It should be noted that the inerter can be seen from the control point of view as a relative acceleration feedback. In other words, subtracted outputs of two accelerometers mounted on the receiving and source bodies could theoretically be fed to the reactive actuator in addition to the existing velocity feedback in order to synthesize the inerter element actively. However, such derivative active vibration control has never been achieved in practice to the best of authors' knowledge. It appears that the corresponding sensor-actuator frequency response function does not roll-off with frequency which causes very pronounced stability problems associated with high frequency poles, as discussed for example in [42]. It is therefore very useful in the present scheme to include the inerter as a passive element which mimics the effects of a relative acceleration feedback to reactive force actuator.

5 Conclusions

In this paper, a novel, inerter-based active vibration isolation system is presented. By investigating the stability of the active control when no inerter is used, it is found that there are two fundamental families of vibration isolation problems. With the first family (supercritical systems), which is characterised by the natural frequency of the uncoupled source body larger than the natural frequency of the uncoupled receiving body, large feedback gains can be used without compromising the stability of the feedback control system. This results in a convincing broadband vibration isolation effect. With the second family of systems (subcritical systems), the natural frequency of the uncoupled source body is below the natural frequency of the uncoupled receiving body. The range of stable feedback gains is limited which results in poor vibration isolation performance. However with the inclusion of the inerter, broadband active vibration isolation can also be achieved in the subcritical family of systems. Adding the inerter into the isolator effectively generates a sort of relative acceleration feedback that stabilises the control loop. In fact, it is analytically calculated in the paper that the minimum inertance to stabilise the loop is proportional to the stiffness of the isolator spring and inversely proportional to the squared natural frequency of the source body. It is important to mention that direct acceleration feedback would not be possible in practice due to very pronounced stability problems, therefore the passive element which mimics such feedback is very useful.

Acknowledgements

This work has been supported by Croatian Science Foundation under the project lP-2019-04-5402.

References

[1] M. C. Smith, “Synthesis of mechanical networks: the inerter,” *IEEE Transactions on Automatic Control*, vol. 47, no. 10, pp. 1648–1662, Oct. 2002.

[2] M. C. Smith and F.-C. Wang, “Performance Benefits in Passive Vehicle Suspensions Employing Inerters,” *Vehicle System Dynamics*, vol. 42, no. 4, pp. 235–257, Dec. 2004.

[3] A. Gonzalez-Buelga, L. R. Clare, S. A. Neild, J. Z. Jiang, and D. J. Inman, “An electromagnetic inerter-based vibration suppression device,” *Smart Materials and Structures*, vol. 24, no. 5, p. 055015, May 2015.

[4] D. De Domenico, P. Deastra, G. Ricciardi, N. D. Sims, and D. J. Wagg, “Novel fluid inerter based tuned mass dampers for optimised structural control of base-isolated buildings,” *Journal of the Franklin Institute*, Nov. 2018.

[5] G. Zhao, G. Raze, A. Paknejad, A. Deraemaeker, G. Kerschen, and C. Collette, “Active tuned inerter-damper for smart structures and its $\mathscr{H}_\infty$ optimisation,” *Mechanical Systems and Signal Processing*, vol. 129, pp. 470–478, 2019.

[6] J. Høgsberg, M. L. Brodersen, and S. Krenk, “Resonant passive-active vibration absorber with integrated force feedback control,” *Smart Materials and Structures*, vol. 25, no. 4, p. 047001, Apr. 2016.

[7] M. Zilletti, “Feedback control unit with an inerter proof-mass electrodynamic actuator,” *Journal of Sound and Vibration*, vol. 369, pp. 16–28, May 2015.

[8] Z. Zhao, R. Zhang, and Z. Lu, “A particle inerter system for structural seismic response mitigation,” *Journal of the Franklin Institute*, vol. 356, no. 14, pp. 7669–7688, 2019.

[9] R. Faraj, Ł. Jankowski, C. Graczykowski, and J. Holnicki-Szulc, “Can the inerter be a successful shock-absorber? The case of a ball-screw inerter with a variable thread lead,” *Journal of the Franklin Institute*, Apr. 2019.

[10] F. Palacios-Quiñonero, J. Rubió-Massegú, J. M. Rossell, and H. R. Karimi, “Design of inerter-based multi-actuator systems for vibration control of adjacent structures,” *Journal of the Franklin Institute*, vol. 356, no. 14, pp. 7785–7809, 2019.

[11] T. Bein, J. Bös, S. Herold, D. Mayer, T. Melz, and M. Thomaier, “Smart interfaces and semi-active vibration absorber for noise reduction in vehicle structures,” *Aerospace Science and Technology*, vol. 12, no. 1, pp. 62–73, Jan. 2008.

[12] I. F. Lazar, S. A. Neild, and D. J. Wagg, “Performance Analysis of Cables with Attached Tuned-Inerter-Dampers,” 2015, pp. 433–441.

[13] I. F. Lazar, S. A. Neild, and D. J. Wagg, “Vibration suppression of cables using tuned inerter dampers,” *Engineering Structures*, vol. 122, pp. 62–71, Sep. 2016.

[14] P. Brzeski, T. Kapitaniak, and P. Perlikowski, “Novel type of tuned mass damper with inerter which enables changes of inertance,” *Journal of Sound and Vibration*, vol. 349, pp. 56–66, Aug. 2015.

[15] P. Brzeski, E. Pavlovskaia, T. Kapitaniak, and P. Perlikowski, “The application of inerter in tuned mass absorber,” *International Journal of Non-Linear Mechanics*, vol. 70, pp. 20–29, Apr. 2015.

[16] Y. Hu and M. Z. Q. Chen, “Performance evaluation for inerter-based dynamic vibration absorbers,” *International Journal of Mechanical Sciences*, vol. 99, pp. 297–307, Aug. 2015.

[17] S. J. Elliott, M. Serrand, and P. Gardonio, “Feedback Stability Limits for Active Isolation Systems with Reactive and Inertial Actuators,” *Journal of Vibration and Acoustics*, vol. 123, no. 2, pp. 250–261, Apr. 2001.

[18] C. Paulitsch, P. Gardonio, and S. J. Elliott, “Active vibration control using an inertial actuator with internal damping,” *The Journal of the Acoustical Society of America*, vol. 119, no. 4, pp. 2131–2140, 2006.

[19] N. Alujević, G. Zhao, B. Depraetere, P. Sas, B. Pluymers, and W. Desmet, “H<inf>2</inf> optimal vibration control using inertial actuators and a comparison with tuned mass dampers,” *Journal of Sound and Vibration*, vol. 333, no. 18, pp. 4073–4083, 2014.

[20] J. Rohlfing, S. J. Elliott, and P. Gardonio, “Feedback compensator for control units with proof-mass electrodynamic actuators,” *Journal of Sound and Vibration*, vol. 331, no. 15, pp. 3437–3450, 2012.

[21] J. Rohlfing, S. J. Elliott, and P. Gardonio, “Compensation Filter for Feedback Control Units with Proof-Mass Electrodynamic Actuators, Simulations and Experimental Studies,” Southampton, 2011.

[22] J. Rohlfing, S. J. Elliott, and P. Gardonio, “Feedback compensator for control units with proof-mass electrodynamic actuators,” *Journal of Sound and Vibration*, vol. 331, no. 15, pp. 3437–3450, Jul. 2012.

[23] G. Zhao, N. Alujević, B. Depraetere, and P. Sas, “Dynamic analysis and <inf>2</inf> optimisation of a piezo-based tuned vibration absorber,” *Journal of Intelligent Material Systems and Structures*, vol. 26, no. 15, pp. 1995–2010, 2015.

[24] G. Zhao, N. Alujević, B. Depraetere, G. Pinte, J. Swevers, and P. Sas, “Experimental study on active structural acoustic control of rotating machinery using rotating piezo-based inertial actuators,” *Journal of Sound and Vibration*, vol. 348, pp. 15–30, 2015.

[25] G. Zhao, N. Alujevia, B. Depraetere, G. Pinte, and P. Sas, “Adaptive-passive control of structure-borne noise of rotating machinery using a pair of shunted inertial actuators,” *Journal of Intelligent Material Systems and Structures*, vol. 27, no. 12, pp. 1584–1599, 2016.

[26] A. Kras and P. Gardonio, “Active vibration control unit with a flywheel inertial actuator,” *Journal of Sound and Vibration*, vol. 464, p. 114987, 2020.

[27] M. Zilletti, P. Gardonio, and S. J. Elliott, “Optimisation of a velocity feedback controller to minimise kinetic energy and maximise power dissipation,” *Journal of Sound and Vibration*, vol. 333, no. 19, pp. 4405–4414, Sep. 2014.

[28] A. Kras and P. Gardonio, “Velocity feedback control with a flywheel proof mass actuator,” *Journal of Sound and Vibration*, vol. 402, pp. 31–50, Aug. 2017.

[29] M. Z. Q. Chen, Y. Hu, C. Li, and G. Chen, “Application of Semi-Active Inerter in Semi-Active Suspensions Via Force Tracking,” *Journal of Vibration and Acoustics*, vol. 138, no. 4, Aug. 2016.

[30] A. Kuznetsov, M. Mammadov, I. Sultan, and E. Hajilarov, “Optimization of improved suspension system with inerter device of the quarter-car model in vibration analysis,” *Archive of Applied Mechanics*, vol. 81, no. 10, pp. 1427–1437, Oct. 2011.

[31] I. F. Lazar, S. A. Neild, and D. J. Wagg, “Using an inerter-based device for structural vibration suppression,” *Earthquake Engineering & Structural Dynamics*, vol. 43, no. 8, pp. 1129–1147, Jul. 2014.

[32] Y. Hu, M. Z. Q. Chen, Z. Shu, and L. Huang, “Analysis and optimisation for inerter-based isolators via fixed-point theory and algebraic solution,” *Journal of Sound and Vibration*, vol. 346, pp. 17–36, Jun. 2015.

[33] A. Caiazzo, N. Alujević, B. Pluymers, and W. Desmet, “Active control of turbulent boundary layer-induced sound transmission through the cavity-backed double panels,” *Journal of Sound and Vibration*, vol. 422, pp. 161–188, 2018.

[34] A. Preumont, *Vibration Control of Active Structures*, vol. 246. Cham: Springer International Publishing, 2018.

[35] C. E. Kaplow and J. R. Velman, “Active Local Vibration Isolation Applied to a Flexible Space Telescope,” *Journal of Guidance, Control, and Dynamics*, vol. 3, no. 3, pp. 227–233, May 1980.

[36] X. Wang, *Vehicle noise and vibration refinement*. CRC Press, 2010.

[37] D. C. Karnopp and A. K. Trikha, “Comparative Study of Optimization Techniques for Shock and Vibration Isolation,” *Journal of Engineering for Industry*, vol. 91, no. 4, pp. 1128–1132, Nov. 1969.

[38] P. Gardonio, M. Gavagni, and A. Bagolini, “Seismic Velocity Sensor With an Internal Sky-Hook Damping Feedback Loop,” *IEEE Sensors Journal*, vol. 8, no. 11, pp. 1776–1784, Nov. 2008.

[39] D. E. Newland, *An introduction to random vibrations, spectral and wavelet analysis*. Dover Publications, 2005.

[40] A. Preumont, A. Francois, F. Bossens, and A. Abu-Hanieh, “Force feedback versus acceleration feedback in active vibration isolation,” *Journal of Sound and Vibration*, vol. 257, no. 4, pp. 605–613, Oct. 2002.

[41] N. Alujević, H. Wolf, P. Gardonio, and I. Tomac, “Stability and performance limits for active vibration isolation using blended velocity feedback,” *Journal of Sound and Vibration*, vol. 330, no. 21, pp. 4981–4997, 2011.

[42] N. Alujević, I. Tomac, and P. Gardonio, “Tuneable vibration absorber using acceleration and displacement feedback,” *Journal of Sound and Vibration*, vol. 331, no. 12, pp. 2713–2728, 2012.